Control Design for a Floating Wind Turbine
Assignment Part I
SC42145 Robust Control

Long Youyuan, 5690641
Qingyi Ren, 5684803
December 2022
Delft University of Technology

December 16, 2022

1 Introduction

In this assignment, we are given the a floating wind turbine system in Fig 1 and required to investigate the controller design methods. Firstly, the floating wind turbine system is nonlinear one, for better analysis, the linearisation is performed at the wind speed $V_{in} = 14m/s$ to obtain linear state-space model:

$$\dot{x} = Ax + Bu \tag{1}$$

$$y = Cx + Du \tag{2}$$

where $x \in \Re^{5\times1}$, $A \in \Re^{5\times5}$, $B \in \Re^{5\times3}$, $u \in \Re^{3\times1}$,$y \in \Re^{2\times1}$, $C \in \Re^{2\times5}$ and $D \in \Re^{2\times3}$. The state vector, input and output of the linearized system are defined as $x = [x_1; x_2; x_3; x_4; x_5]$, $u = [\beta; \tau_e; V]$ and $y = [w_r; z;]$, and matrices A, B, C and D are given in MATLAB file. Secondly, the model has three inputs, which is stacked in the vector u, including blade pitch angle β [rad], the generator torque τ_e $[N \cdot m]$ and the wind speed V [m/s] which is the derivation from from the linearisation point (β and τ_e are the control inputs of system and V is the disturbance input of the system). Then generator speed w_r [rad/s] and the fore-aft tower top displacement Z [m] are taken as the output of the system, which composing the output vector y. Finally the fore-aft tower top displacement Z can be decomposed as $Z = Z_1 + Z_2$ where Z_1 and Z_2 represent tower bending and platform tilting modes respectively, shown in Fig 2. The state vector $x = [x_1; x_2; x_3; x_4; x_5]$ describes dynamics of the system $x_1 = w_r$, $x_2 = \dot{z_1}$, $x_3 = z_1$, $x_4 = \dot{z_2}$ and $x_5 = z_2$.

Figure 1: An example of a Floating Wind Turbine (FWT).

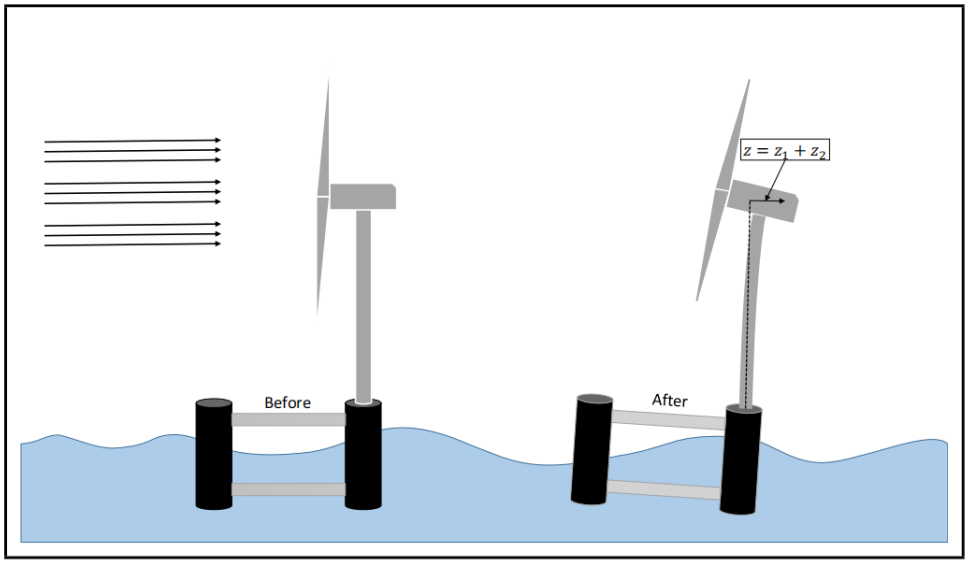

Figure 2: Schematic depiction of fore-aft movement.

2 SISO Analysis and Control Design

In this section, it is required to design SISO controller for the float wind turbine system in scenario where use blade pitching to increase

the rotational velocity of the turbine and obtain new desired generator speed. The transfer function of the float wind turbine system is firstly acquired as:

```
%% Part 1-1 SISO Analysis and Control Design
clear; clc; close all;
load('Assignment_Data_SC42145_2022');
s =tf ('s');
G=ss(A,B,C,D);
G1=tf(G);
```

The float wind turbine system is MIMO system, having three inputs and two outputs, the transfer function can be written as

$$G1 = \begin{bmatrix} G_{11} & G_{12} & G_{13} \\ G_{21} & G_{22} & G_{23} \end{bmatrix}$$

In Fig3, it shows the structure and values of transfer function $G1$, the required SISO system which takes β as input and w_r as output has the transfer function

$$G_S = -G_{11} = \frac{0.07988s^4 + 0.003315s^3 + 0.8677s^2 - 0.006493s + 0.03458}{s^5 + 0.5979s^4 + 10.98s^3 + 4.709s^2 + 0.5421s + 0.1827} \tag{3}$$

(G_{11} multiplied with -1), which represents the mapping relation from input $u_1 = \beta$ to output $y_1 = w_r$.

2.1 Open-Loop analysis

In order to choose proper type of controller, one is required to analyse the properties of open-loop system. The open-loop bode plot and pole-zero map of the plant are shown in Figs 4 and 5.

From the pole-zero map of the plant and table 1, we obtain that there is no poles on the right-half plane, however there exist a pair of complex zeros $zero_1 = 0.0038 + 0.2i$ and $zero_2 = 0.0038 - 0.2i$ in the right-half plane which limit the bandwidth frequency. Then the limitations imposed by RHP-zero on bandwidth is written as: $\left|\frac{z/M+w_B}{z+w_B A}\right| < 1$. Because RHP zeros are a pair of complex values, in the form of $zeros = x \pm yi$, where $x = 0.0038$ and $y = 0.2$, the maximum attainable bandwidth frequency is computed as

$$w_B^* = -\frac{x}{M} + \sqrt{x^2 + y^2(1 - \frac{1}{M^2})} \tag{4}$$

```
>> G1

G1 =

  From input 1 to output...
       -0.07988 s^4 - 0.003315 s^3 - 0.8677 s^2 + 0.006493 s - 0.03458
   1:  ------------------------------------------------------------------
        s^5 + 0.5979 s^4 + 10.98 s^3 + 4.709 s^2 + 0.5421 s + 0.1827

              -0.04874 s^3 - 0.03481 s^2 - 0.07497 s - 0.052
   2:  ------------------------------------------------------------
       s^5 + 0.5979 s^4 + 10.98 s^3 + 4.709 s^2 + 0.5421 s + 0.1827

  From input 2 to output...
       -0.009564 s^4 - 0.001683 s^3 - 0.1039 s^2 - 0.001187 s - 0.00414
   1:  ------------------------------------------------------------------
         s^5 + 0.5979 s^4 + 10.98 s^3 + 4.709 s^2 + 0.5421 s + 0.1827

                  -0.001614 s^2 - 2.522e-05 s - 0.002465
   2:  ------------------------------------------------------------
       s^5 + 0.5979 s^4 + 10.98 s^3 + 4.709 s^2 + 0.5421 s + 0.1827

  From input 3 to output...
       0.2204 s^4 + 0.02348 s^3 + 2.394 s^2 + 0.003981 s + 0.09541
   1:  ------------------------------------------------------------
       s^5 + 0.5979 s^4 + 10.98 s^3 + 4.709 s^2 + 0.5421 s + 0.1827

              0.06941 s^3 + 0.06756 s^2 + 0.1071 s + 0.1015
   2:  ------------------------------------------------------------
       s^5 + 0.5979 s^4 + 10.98 s^3 + 4.709 s^2 + 0.5421 s + 0.1827

Continuous-time transfer function.
```

Figure 3: Transfer function $G1$ of the the float wind turbine system.

when $t \to \infty$, the $\lim_{M\to\infty} w_B^* = \sqrt{x^2+y^2} \approx y = 0.2$ [rad/s]. In order to illustrate the limitation of maximum attainable bandwidth frequency caused by RHP zeros, the PID controller is designed and connected with plant G_S in series connection. By using different values of parameter K_I, the open-loop bode lines of system with different values of PID controller parameter P_I have different shapes, but all the lines drop large phase at maximum attainable bandwidth frequency 0.2 rad/s. It will lead to the bad performance when having the input signal with higher frequency than bandwidth frequency. More specifically, the system will not be able to perform reference tracking in normal amplitude when input signal is of high frequency larger than 0.2 rad/s, which cannot be enhanced by regulating PID parameters. Also if the bandwidth is relatively small, the system will respond sluggishly and has higher values of rise time and settling time but have higher robustness against disturbance.

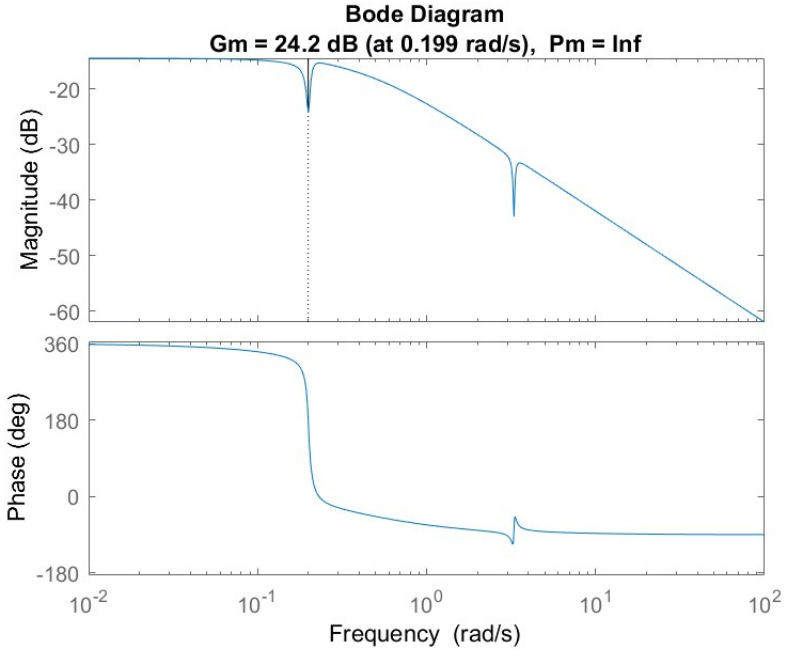

Figure 4: Open-loop bode plot.

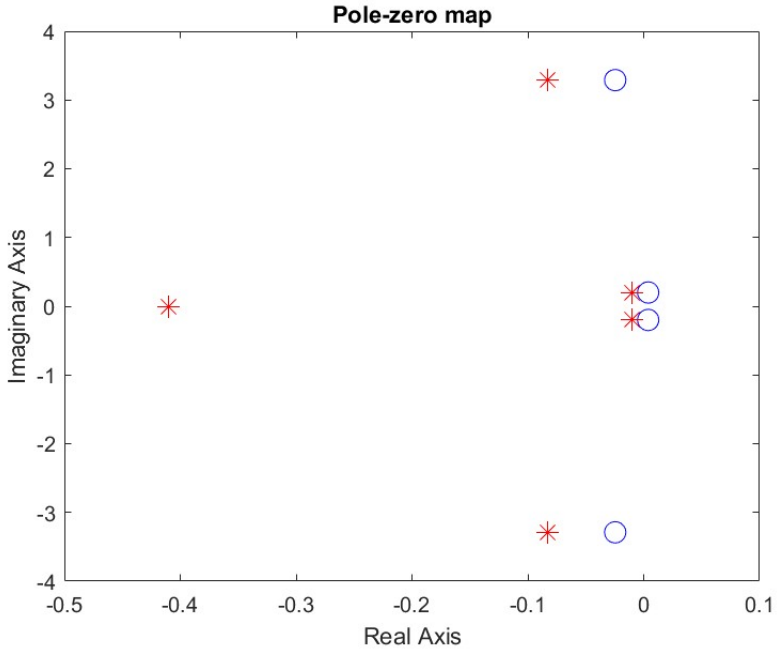

Figure 5: Pole-zero map of the plant.

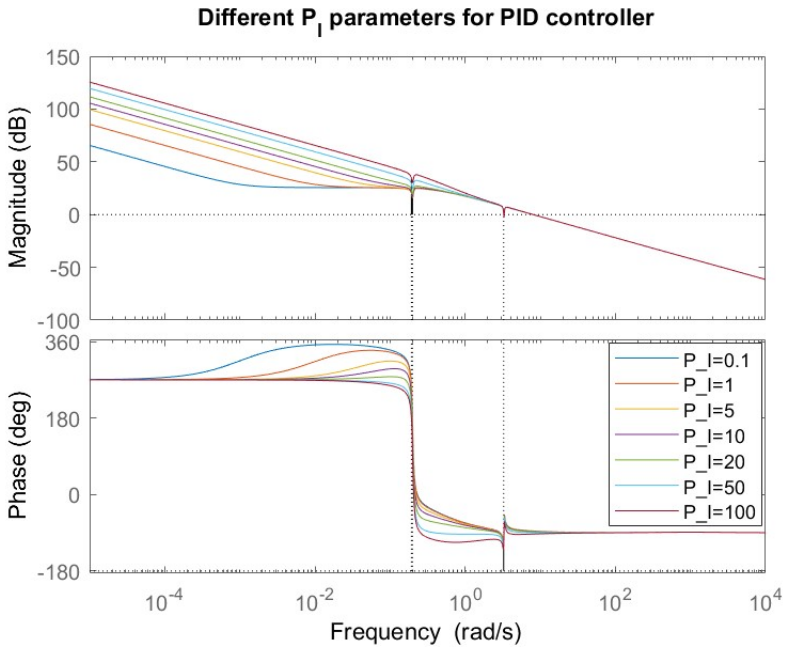

Figure 6: Open-loop bode graph of system plugged in PID controller with different values of P_I parameter.

zeros	position
1	-0.0246 + 3.2897i
2	-0.0246 - 3.2897i
3	0.0038 + 0.2i
4	0.0038 - 0.2i
poles	position
1	-0.4103
2	-0.0833 + 3.2942i
3	-0.0833 - 3.2942i
4	-0.0105 + 0.2022i
5	-0.0105 - 0.2022i

Table 1: The location of zeros and poles of G_S.

2.2 SISO controller design

The SISO controller is designed to satisfy three design requirements:

(a) Small settling-time

(b) overshoot $< 1\%$

(c) steady-state error = 0

In order to design controller properly, sometimes we need to analyze the the properties of system in time-domain and frequency-domain and find the relationship between the time-domain and frequency-domain control requirements. Firstly, the overshoot is given as less than 1%. The classical method is to approximate the control system as protocol second-order system, which is not applicable to our SISO system of fifth-order and type 0. Inspired of different shapes of open-loop bode of system plugged in PID controller with different values of P_I parameter, the step response of system shown in Fig 6 is also obtained to compare with frequency performance of system. In table 2, it is clearly show the negative

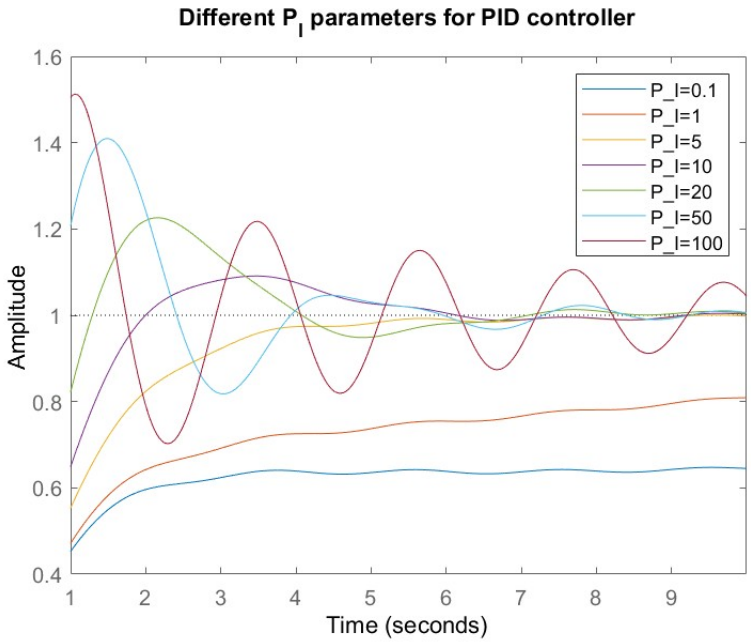

Figure 7: The step response of system plugged in PID controller with different values of P_I parameter.

correlation between the overshoot and phase margin: the higher the overshoot the lower the phase margin. The rise time and gain margin, overshoot and crossover frequency, phase margin and gain margin, crossover frequency and settling time have positive correlation. In order to obtain small settling time, we can make the system have lower crossover frequency, by the way of decreasing K_P and K_I of PID controller. However, if K_P is set too small, the system will

PID	Time-domain			Frequency-domain		
K_I	OS[%]	RT[s]	ST[s]	COF[rad/s]	PM[°]	GM[dB]
0.1	0.8602	149.5301	607.7782	0.1929	76.9824	1.6141
1	3.5388	15.6612	643.2010	0.1945	40.4103	1.3432
5	0	NAN	NAN	0.8338	86.8286	0.4032
10	9	NAN	NAN	1.0310	68.5552	0.1913
20	22.5883	0.9969	5.9592	1.3569	51.2313	0.0916
50	40.8974	0.6057	7.9784	2.0511	32.3758	0.0355
100	51.1565	0.4152	19.6789	2.8323	18.0522	0.0176

Table 2: Comparision between time-domain and frequency-domain of system's performance. Note that: OS, RT, ST, COF, PM and GM are shortened form of overshoot, rise time, settling time, crossover frequency, phase margin and gain margin respectively.

have slow response and the feedback performance is week. Similarly, if K_I is set too small, the system will respond slowly and the step response will become non-oscillatory process. Thus PID controller design method is required to comprehensively consider various control design requirements.

From the open-loop bode plot in Fig4, it was observed that the SISO system has two notches, which can be eliminated by using the notch filers respectively, C_{notch1} and C_{notch2}.

$$C_{notch} = \frac{s^2 + 2w\beta_1 s + w^2}{s^2 + 2w\beta_2 s + w^2} \tag{5}$$

In controllers C_{notch1} and C_{notch2}, the parameters $w_1 = 0.2$ [rad/s] and $w_2 = 3.29$ [rad/s] which are obtained in the Fig 4, and β_1 and β_2 are chosen as 5 and 100 by using trial-and-error method.

The steady state error of close-loop system can be computed as:

$$\begin{aligned} e(\infty) &= \lim_{t\to\infty} e(t) = \lim_{s\to 0} sE(s) = \lim_{s\to 0} s\frac{R(s)}{1+G_S(s)} = \lim_{s\to 0}\frac{1}{1+G_S(s)} \\ &= \frac{1}{1+\frac{0.07988s^4+0.003315s^3+0.8677s^2-0.006493s+0.03458}{s^5+0.5979s^4+10.98s^3+4.709s^2+0.5421s+0.1827}} = 0.8409 \end{aligned}$$

Here we use step input $R(s) = \frac{1}{s}$. It can be observed that the system is type 0 and has non-zero steady error, thus integral action for the reference tracking is necessary, which means that controller structure need to be chosen from PI and PID. The derivative element is also needed because around 360 degree phase drops around the frequency

$0.199 rad/s$ shown in Fig 4. The general approach of phase increase is derivative element. For the summation, the SISO controller is chosen in the type of PID in consideration of eliminating steady error and loop shaping.

In this assignment, Ziegler -Nichols method is used to regulate proper PID parameters, which contains fours steps:

(1) Connect the PID controller in the open-loop and set all parameters to zero.

(2) Gradually increase K_P to the extent that the response to disturbance is the shape of oscillation.

(3) When system has equal amplitude oscillation, takes the gain value as critical gain K_u and the period time as critical period T_u.

(4) Finally get the proper PID parameters as $K_P = 0.6K_u$, $K_I = 0.5T_u$ and $K_D = 0.125T_u$.

Following the former steps, the parameters for PID controller are shown in Table 3. Connecting the two notch filters C_{notch1}, C_{notch2} and PID controller C_{PID} in serial, the overall controller is designed as $C = C_{notch1}C_{notch2}C_{PID}$ and now the open-loop transfer function is $OL = C_{notch1}C_{notch2}C_{PID}G_S$.

$$C_{PID} = K_P + \frac{K_I}{s} + \frac{K_D s}{T_f s + 1} \tag{6}$$

PID parameters	
K_P	100
K_I	82
K_D	5
T_f	1000

Table 3: PID parameters.

2.3 Implementing SISO controller and performance analysis

In this section, the SISO controller is designed properly and analysed performance in time domain and frequency respectively. The close-loop step response, open-loop bode graph and close-loop bode graph

are shown in Figs 8, 9 and 10, which illustrate the time-domain and frequency-domain characteristics. In table 4, it lists the SISO system's properties of time-domain and frequency-domain. Note that the bandwidth of SISO system is approximately to the frequency value of the magnitude $-3dB$ at the bode graph of close-loop transfer function, which is shown in Fig 10, around the value $0.0572rad/s$.

Compared with requirements of controller design requirements mentioned before, the SISO controller satisfies the all the control targets but still has some problems with limitation of bandwidth at $0.0572rad/s$, which means that when reference signal is higher than bandwidth frequency, SISO system will not be able to perform reference tracking in normal amplitude which cannot be enhanced by regulating PID parameters. If the bandwidth is small, although the SISO system responds sluggishly and has higher values of rise time and settling time, it has higher robustness. If the bandwidth is large, high-frequency signals are easily transformed to the outputs which makes the system respond quickly to the reference signal, i.e., have small rise time at the cost of higher sensitivity to noise. From former analysis, RHP zeros account for the low bandwidth of the system, the maximum attainable bandwidth frequency is $0.2rad/s$. Another problem is not able to properly design notch filer, even trying so many pairs of β_1 and β_2 still there exist notches left in open-loop and close-loop bode graphs of SISO systems, this may cause negative amplitudes and damps around the time interval $[0, 0.1]\,s$.

Time domain characteristics	
Rise time	45.8s
Settling time	83.2s
Overshoot	0.98%
Steady error	0
Frequency domain characteristics	
Crossover frequency	0.193 rad/s
Bandwidth	0.0572 rad/s
Phase margin	84.2°
Gain margin	17.2 dB

Table 4: Time-domain and frequency-domain of system's performance.

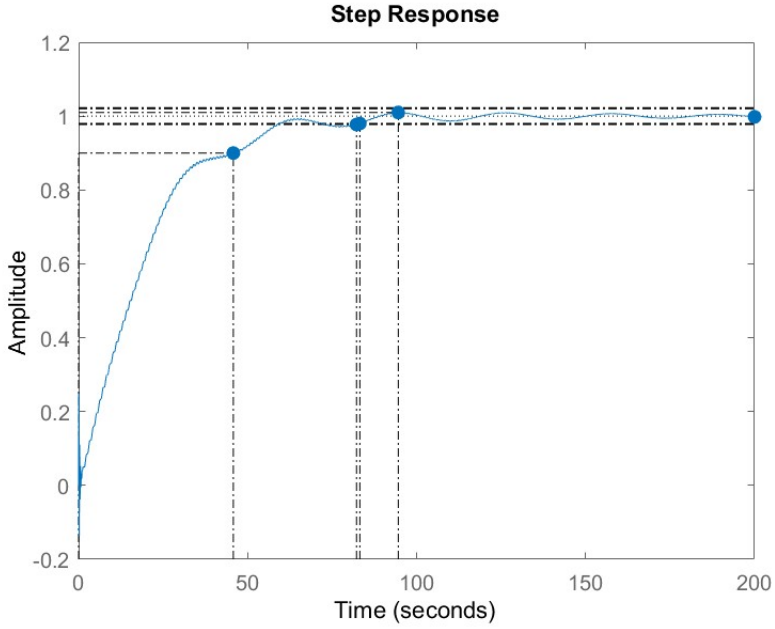

Figure 8: The close-loop step response.

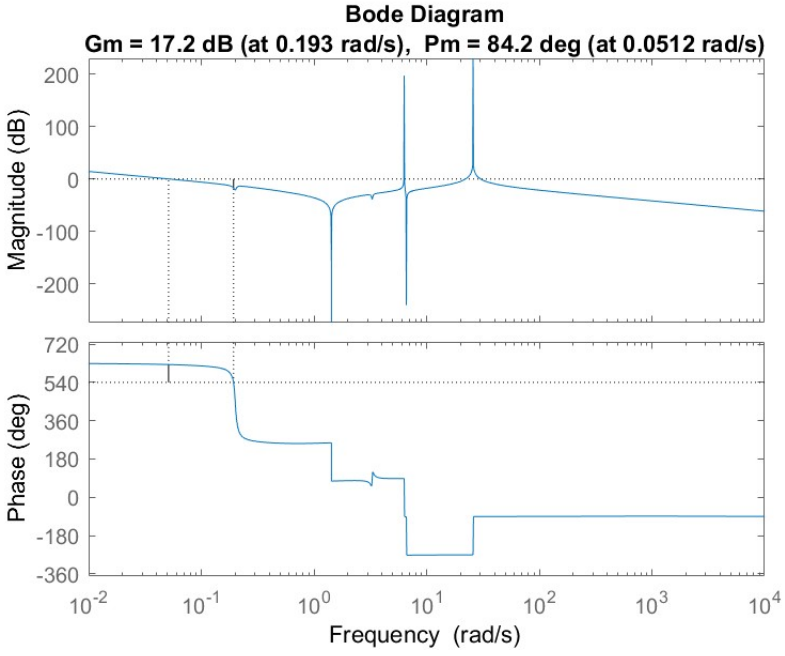

Figure 9: The open-loop bode graph.

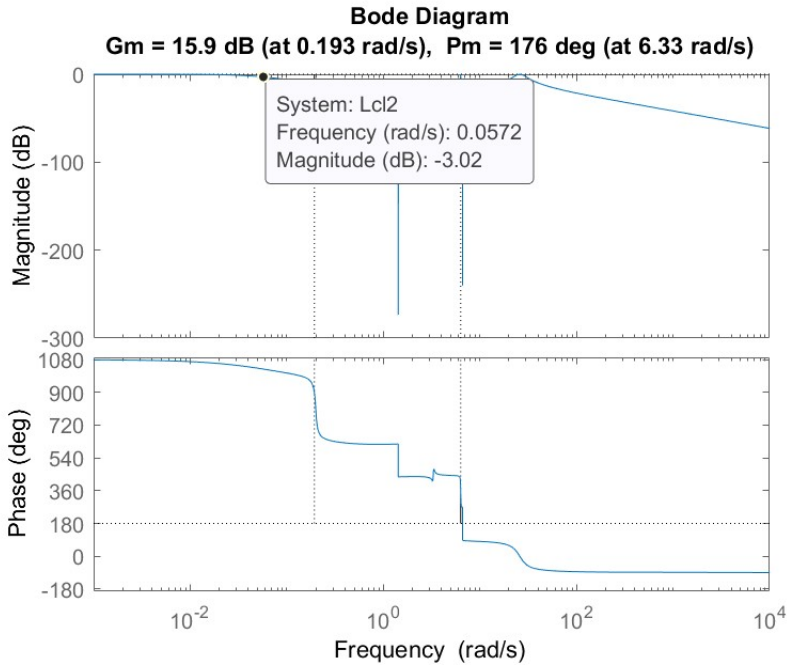

Figure 10: The close-loop bode graph.

2.4 Disturbance rejection

In this part we use SISO controller for rejecting output disturbance shown in Fig 11. The relationship between the output y and reference r and disturbance d is written in the equation (7). The rejection model has two inputs reference r and disturbance d, in order to rejecting output disturbance, in order to eliminate influence of the disturbance on the output, reference r needs to be set to zero, in another word, we only need to analyse the $y = y_2 = (I+GK)^{-1}G_d d$.

$$\begin{aligned} y &= y_1 + y_2 = (I+GK)^{-1}GKr + (I+GK)^{-1}G_d d \\ y_1 &= (I+GK)^{-1}GKr \\ y_2 &= (I+GK)^{-1}G_d d \end{aligned} \tag{7}$$

Then the SISO controller is used as the controller K in Fig 11, G and G_d corresponds to transfer functions G_S and

$$G_d = G_{13} = \frac{0.2204s^4 + 0.02348s^3 + 2.394s^2 + 0.003981s + 0.09541}{s^5 + 0.5979s^4 + 10.98s^3 + 4.709s^2 + 0.5421s + 0.1827} \tag{8}$$

Because the controller K, G and G_d are all one-dimensional, the close-loop transfer function of disturbance rejection model can be

written as:

$$Y(s) = \frac{G_d(s)}{1 + G_S(s)C(s)} D(s) \tag{9}$$

According to equation (9), the time response of output y with the step input d is presented in Fig 12, from which it is observed that the SISO controller is not that suitable for disturbance rejection model, with undesired large overshoot value and settling time. Increasing the parameters K_P and K_I can enhance these properties to some extent, for example, when $K_P = 600$ and $K_I = 200$, the time response of step input d is shown in Fig 13. Compared with two step response of step input d, the enhanced system has better performance of lower overshoot and settling time.

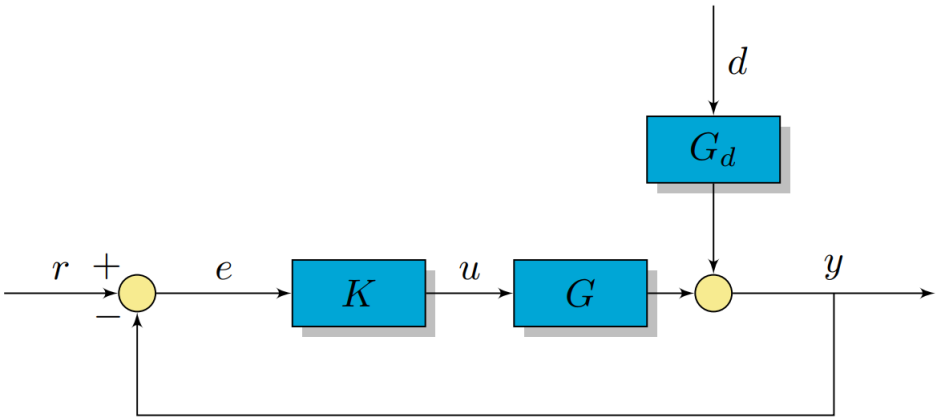

Figure 11: Disturbance rejection model.

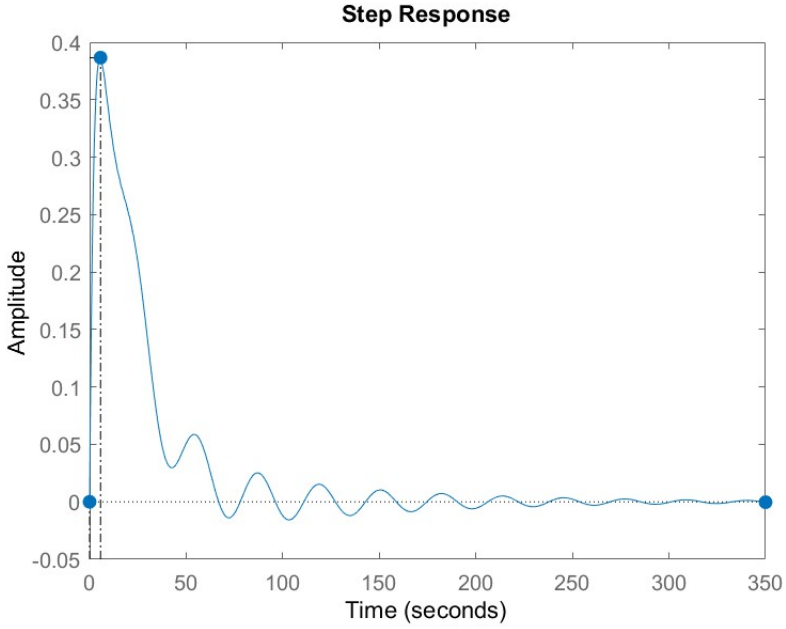

Figure 12: Time response of step input of disturbance d.

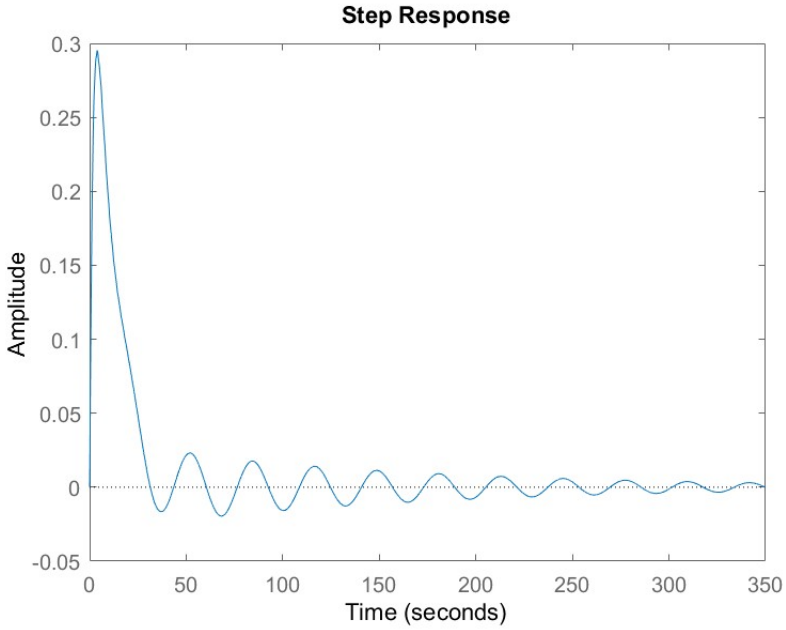

Figure 13: Enhanced time response of step input of disturbance d.

3 Multi variable Mixed-Sensitivity

In this section, we will explore Mixed-Sensitivity centralized controller. Starting from this part, the focus will be put on MIMO system, which takes both channels, blade pitch angle β and generator torque τ_e, as inputs of systems.

3.1 RGA

$\omega = 0$ and $\omega = 0.3 \times 2 \times \pi$ is shown below.

$$\begin{aligned} RGA_{\omega=0} &= \begin{bmatrix} -0.6554 & 1.6554 \\ 1.6554 & -0.6554 \end{bmatrix} \\ RGA_{\omega=0.3\times2\times\pi} &= \begin{bmatrix} -0.1166 & 1.1166 \\ 1.1166 & -0.1166 \end{bmatrix} \end{aligned} \tag{10}$$

The RGA is introduced as a steady-state measure of interactions for decentralized control, which is described in 11.

$$RGA(G) = \Lambda(G) \triangleq G \times (G^{-1})^T \tag{11}$$

Relative gain λ_{ij} indicates the influence level to the control from input u_j to output y_i by other close loops. If $\lambda_{ij} = 1$, it means the control from input u_j to output y_i does not be affected by other loops. Therefore, the variables with an RGA of 1 are preferred to be paired. When the value of λ_{ij} is farther from 1, it means this close loop is easier to be affected by other loops. If $\lambda_{ij} < 0$, it means negative coupling and pairing on negative steady-state RGA elements will result in instability, so it should be avoided.

In this case, the diagonal elements are all negative for both frequencies, while the off diagonal elements are positive, and moreover, they are almost identity at the crossover frequency, namely, $\omega = 0.3 \times 2 \times \pi$. Therefore, (β, z) and (τ_e, ω_r) shoulded be paired.

3.2 MIMO poles and zeros

The MIMO poles and zeros are shown in figure 14. There are no RHP zeros or poles, which means that the system is stable and no consideration is needed for limitations on performance in the MIMO system.

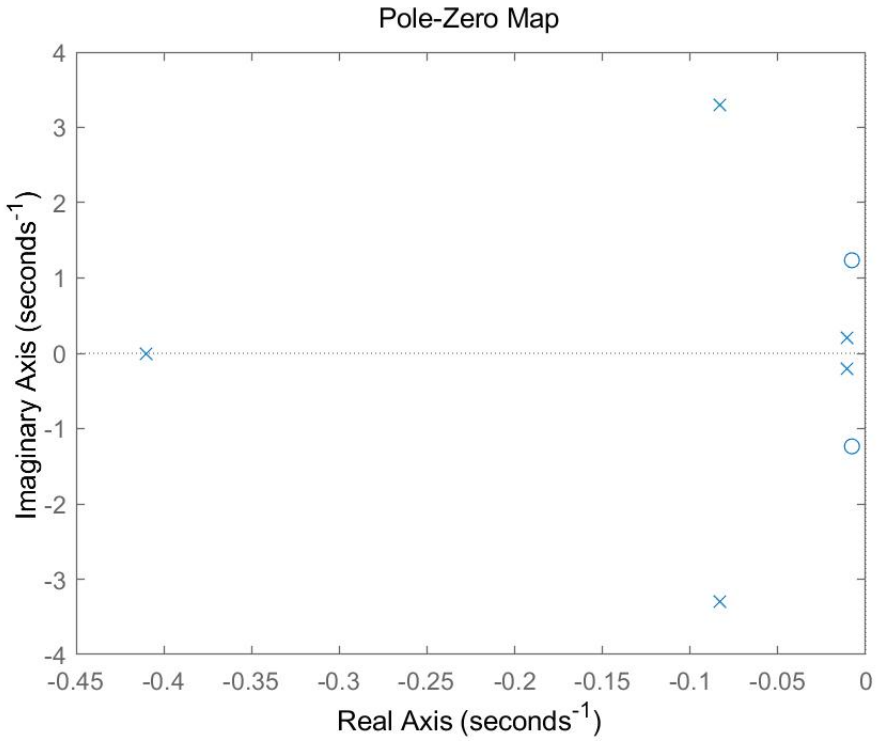

Figure 14: MIMO poles and zeros

zeros	position
1	-0.0078 + 1.2358i
2	-0.0078 - 1.2358i
poles	position
1	-0.4104
2	-0.0832 + 3.2936i
3	-0.0832 - 3.2936i
4	-0.0106 + 0.2022i
5	-0.0106 - 0.2022i

Table 5: MIMO poles and zeros

3.3 Weighted sensitivity design

The weight W_{p11} that be chosen can be represented as below.

$$W_{p11} = \frac{\frac{s}{M} + \omega_B^*}{s + \omega_B^* A} \tag{12}$$

At low frequencies, $|W_{p11}(j\omega)|^{-1}$ is equal to A, is equal to M at high frequencies, and also asymptotically crosses 1 at frequency ω_B^*, so ω_B^* can be regarded as cut-off frequency of $|W_{p11}(j\omega)|^{-1}$.

Therefore, According to the question, to get a cut-off frequency of 0.3Hz, we choose $\omega_B^* = 0.3Hz = 0.3 \times 2\pi$; to get an attenuation of low-frequency disturbances of 10^{-4}, A should be equal to 10^{-4}; and to get an H_∞ norm of the sensitivity function of 3, M is designed as 3. Finally, we get the formula of W_{p11} as:

$$W_{p11} = \frac{\frac{s}{3} + 0.3 \times 2\pi}{s + 0.3 \times 2\pi \times 10^{-4}} \tag{13}$$

3.4 Block diagram

The block diagram is shown in figure 15.

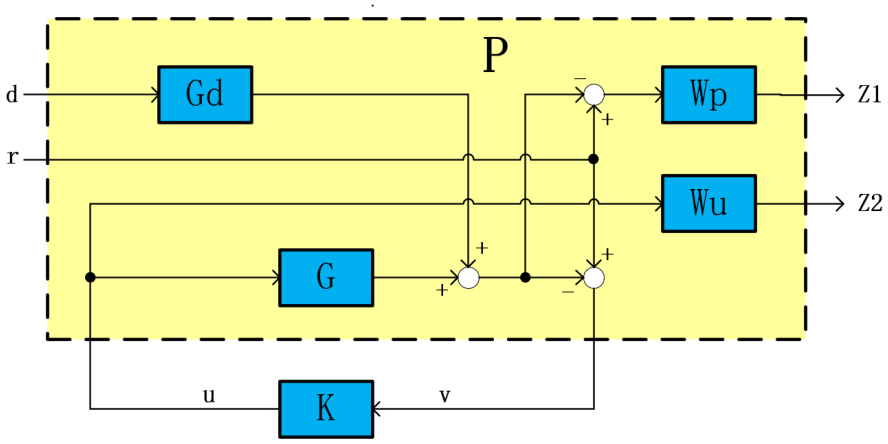

Figure 15: Model of the floating wind turbine and controller with mixed sensitivity.

In this block diagram:

(1) d and r are 1-dimension and 2-dimension exogenous inputs respectively.

(2) G, K, W_p and W_u are 2×2 transfer function matrix.

(3) Gd is a 2×1 transfer function matrix.

(4) z_1, z_2 are 1-dimension and 2-dimension exogenous outputs.

(5) u and v are 2-dimension control signals and output signals respectively.

3.5 Derivation of a generalized plant

From figure 15, we can get following equations of generalized plant:

$$\begin{aligned} z_1 &= W_p(r - G_d d - Gu) \\ z_2 &= W_u u \\ v &= r - G_d d - Gu \end{aligned} \tag{14}$$

The generalized plant P from input $[d, r, u]^T$ to output $[z_1, z_2, v]^T$ is defined as:

$$P = \left[\begin{array}{cc|c} -W_p G_d & W_p & -W_p G \\ 0 & 0 & W_u \\ \hline -G_d & I_{2\times 2} & -G \end{array}\right] \tag{15}$$

3.6 Interpretation to the given performance weights

3.6.1 Interpretation to W_p

From 16, it can be noticed that sensitivity function can reflect the impact of disturbance to output and every element of sensitivity function shows the impact from $G_d d$ to y at a certain channel.

$$y = (I + GK)^{-1} G_d d = S G_d d \tag{16}$$

The sensitivity weight sets a upper bound to each element of sensitivity function, which can be shown in 17.

$$W_p S = \begin{bmatrix} W_{p11} & 0 \\ 0 & 0.2 \end{bmatrix} \begin{bmatrix} S_{11} & S_{12} \\ S_{21} & S_{22} \end{bmatrix} = \begin{bmatrix} W_{p11} S_{11} & W_{p11} S_{12} \\ 0.2 S_{21} & 0.2 S_{22} \end{bmatrix} \tag{17}$$

From figure 16, the sensitivity weight W_{p11} shows a high penalty to the channels from disturbance to output ω_r at low frequency, which can help reject low-frequency disturbance at output ω_r efficiently. Because of the limitation of sensitivity, at high frequency, W_{p11} sets a upper bound around 14db to S_{11} and S_{12}. While the down-right element of W_p set a upper bound around 14 db at all frequency to S_{21} and S_{22} (the same as W_{p11} at high frequency), which means low penalty to the channels from disturbance to second output z at all frequency. This is because the output z does not matter in this design.

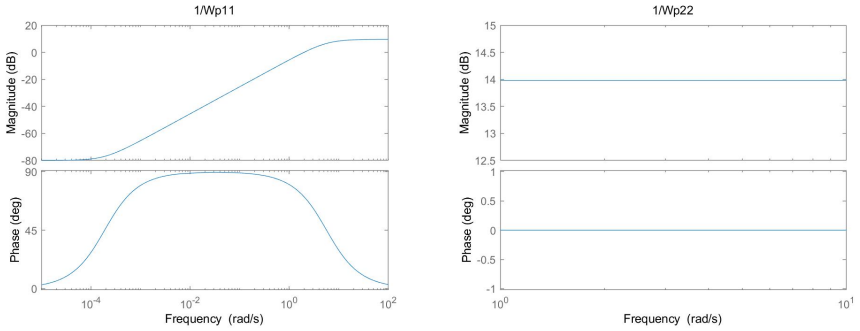

(a)$1/W_{p11}$. (b)$1/W_{p22}$

Figure 16: bode diagram:$\frac{1}{W_{p11}}$ and $\frac{1}{W_{p22}}(1/0.2)$.

3.6.2 Interpretation to W_u

The equation 18 shows how the input r and disturbance $G_d d$ influence the controller output u. In this design, the second controller output τ_e should converge to zero after input and disturbance becoming constant to make sure the power production unchanged.

$$u = KS(r - G_d d) \tag{18}$$

Similar to previous analysis, every element of KS shows the impact from input(or disturbance) to controller output at a certain channel, and the weight W_u also sets a boundary to KS.

$$W_u KS = \begin{bmatrix} 0.01 & 0 \\ 0 & W_{u22} \end{bmatrix} \begin{bmatrix} KS_{11} & KS_{12} \\ KS_{21} & KS_{22} \end{bmatrix} = \begin{bmatrix} 0.01KS_{11} & 0.01KS_{12} \\ W_{u22}KS_{21} & W_{u22}KS_{22} \end{bmatrix} \tag{19}$$

From the figure17, W_{u22} shows a high penalty at low frequency. Combined with equation 19, the result showing that the gain from input and disturbance to the controller output τ_e is highly attenuated at low frequency, which can guarantee that it has no static contribution ($\lim_{t\to\infty} \tau_e(t) = 0$). By contrary, looking at W_{u11}, it sets a high upper bound to KS_{11} and KS_{12}, which means the input and disturbance can influence the controller output β arbitrarily, as there is no specific design requirement to this controller output.

3.7 Mixed-sensitivity generalized controller design

3.7.1 controller design

We use following matlab code to design the controller.

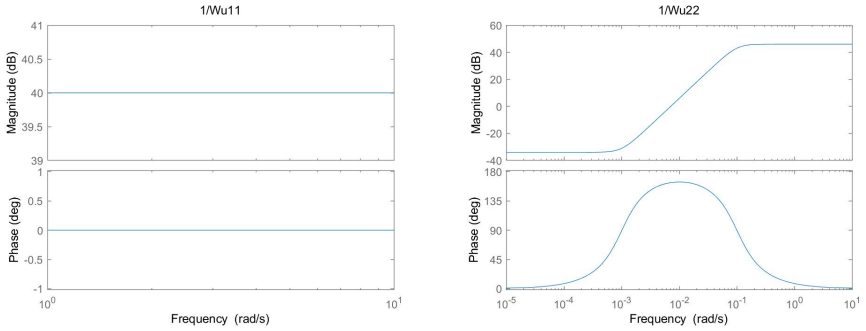

(a)$1/W_{u11}$. (b)$1/W_{u22}$

Figure 17: bode diagram:$\frac{1}{W_{u11}}$ and $\frac{1}{W_{u22}}(1/0.01)$.

```
%% Part 2 mixed-sensitivity generalized controller
    design
clear all; clc;close all;
load('Assignment_Data_SC42145_2022.mat');
FWT_tf = tf(FWT);
G = FWT_tf(1:2,1:2);
s=tf('s');
wB1 = 0.3*2*pi;
A = 1/10000;
M = 3;
Wp=[(s/M+wB1)/(s+wB1*A) 0; 0 0.2];
Wu = [0.01 0;0 (5e-3*s^2+7e-4*s+5e-5)/(s^2+14e-4*s+1e
    -6)];
systemnames = 'G Wp Wu Gd'; % Define systems
inputvar = '[d(1); r(2); u(2)]'; % Input generalized
    plant
input_to_G = '[u]';
input_to_Wu = '[u]';
input_to_Gd= '[d]';
input_to_Wp = '[r-Gd-G]';
outputvar = '[Wp;Wu;r-G-Gd]'; % Output generalized
    plant
sysoutname= 'P';
sysic;
[K,CL,GAM,INFO] = hinfsyn(P,2,2); % Hinf design
K = minreal(K);
```

The state space of the controller K that we get with the code above is shown below.

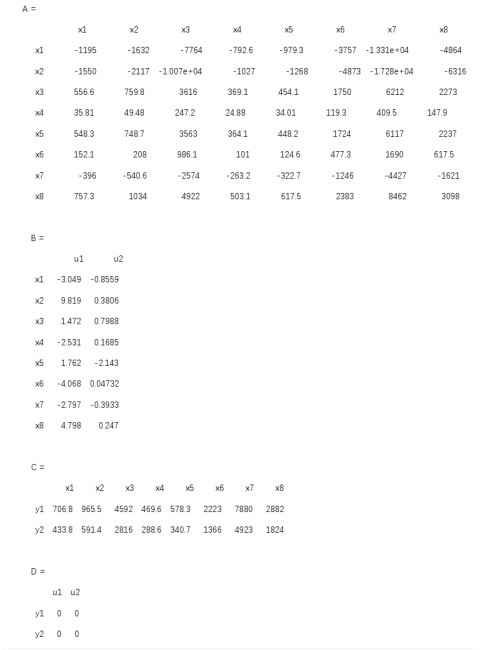

A =

	x1	x2	x3	x4	x5	x6	x7	x8
x1	-1195	-1632	-7764	-792.6	-979.3	-3757	-1.331e+04	-4864
x2	-1550	-2117	-1.007e+04	-1027	-1268	-4873	-1.728e+04	-6316
x3	556.6	759.8	3616	369.1	454.1	1750	6212	2273
x4	35.81	49.48	247.2	24.88	34.01	119.3	409.5	147.9
x5	548.3	748.7	3563	364.1	448.2	1724	6117	2237
x6	152.1	208	986.1	101	124.6	477.3	1690	617.5
x7	-396	-540.6	-2574	-263.2	-322.7	-1246	-4427	-1621
x8	757.3	1034	4922	503.1	617.5	2383	8462	3098

B =

	u1	u2
x1	-3.049	-0.8559
x2	9.819	0.3806
x3	1.472	0.7988
x4	-2.531	0.1685
x5	1.762	-2.143
x6	-4.068	0.04732
x7	-2.797	-0.3933
x8	4.798	0.247

C =

	x1	x2	x3	x4	x5	x6	x7	x8
y1	706.8	965.5	4592	469.6	578.3	2223	7880	2882
y2	433.8	591.4	2816	288.6	340.7	1366	4923	1824

D =

	u1	u2
y1	0	0
y2	0	0

Figure 18: State space of controller.

3.7.2 internally stability analysis

To check the internally stability of the system, generalized Nyquist method is used here. Firstly, figure 19 is the Nyquist plot of transfer function $det(I - L(s))$, where the L(s) the the open loop transfer function of the system, which is equal to $G(s)*K(s)$. When zooming in this plot at origin point, the figure 20 is acquired. From figure 20, it is concluded that the contour map of $det(I - L(s))$ encircles origin **-2** times clockwise.

Secondly, with matlab, it can be calculated that the transfer function $L(s)$ has **two** RHP poles, which are $0.0221 \pm 3.5415i$.

$$det(I + L(s)) = c \cdot \frac{Closed\ Lp\ characteristic\ polynomial}{Open\ Lp\ characteristic\ polynomia} \tag{20}$$

Based on formula 20 and Cauchy's argument principle, the conclusion that there is no unstable closed loop poles of the system can be reached. Therefore, the system is internally stable (because when looking at other input-output channels, the open loop tf L(s) does not change, same result about stability can be reached).

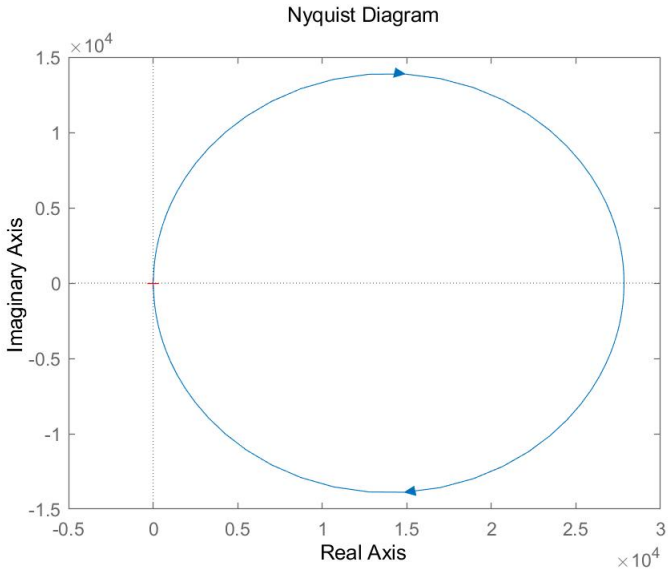

Figure 19: Generalized Nyquist plot of det(I-L(s)).

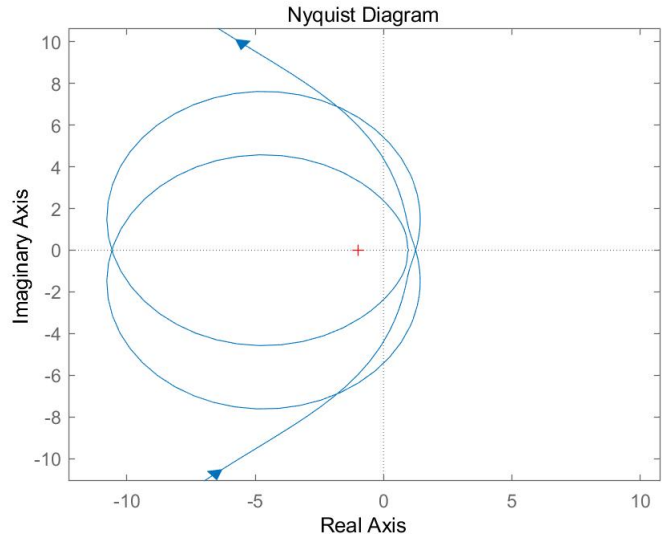

Figure 20: Generalized nyquist plot:Zoom at origin.

3.7.3 states of the controller and plant

In figure 18, the A matrix is 8×8, which means the controller has **8** states. From figure 15, the generalized plant consists of W_p, W_u G_d *and* G. W_p, W_u has 1 and 2 states respectively and

G_d , G commonly has 5 states. Overall, the generalized plant has **8** states totally.

3.8 Time-domain simulation

The system structure implemented performance weights in the simulink is shown in figure 21. The expectation is to keep the power production $P_o = \tau_e \times \omega_r$ unchanged. However, from figure 23, when the disturbance appears, the controller output τ_e shows a massive change to cancel out the influence of the transient change of disturbance and converge to zero until the disturbance become steady (the impact of steady disturbance will be eliminated by controller output β), which takes long time, nearly 400 seconds. In real situations, the disturbance exists all the time and maybe changes with time. This means the controller output τ_e will need to show a big oscillation to keep output ω_r stable at 0. Therefore, it is hard to make sure the unchanged power production. Besides, from figure 22, it is also noticed that a step reference can also result in big oscillation on the controller output τ_e. As shown in figure 24, the reference changes periodically, the controller output τ_e shows a massive and constant oscillation.

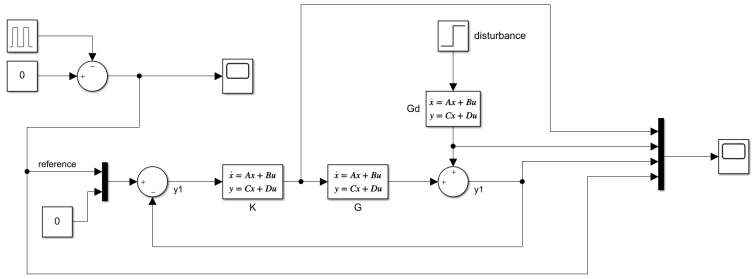

Figure 21: system structure.

4 MIMO Weighting Design

In this section, there are two parts of MIMO weighting design based on controller sensitivity function (KS) and sensitivity function (S). The change in rotational velocity w_r can be compensated by a derivation in either blade pitch angle β or generator torque τ_e. Considering the characteristics of the two inputs and the influence on

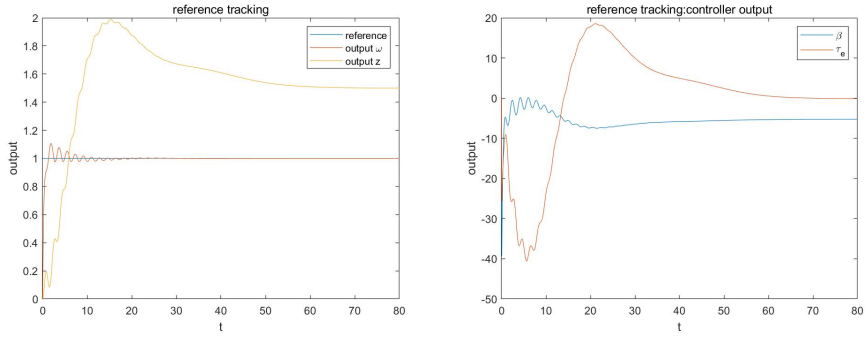

(a)reference and FWT output signals (b)controller output

Figure 22: reference tracking.

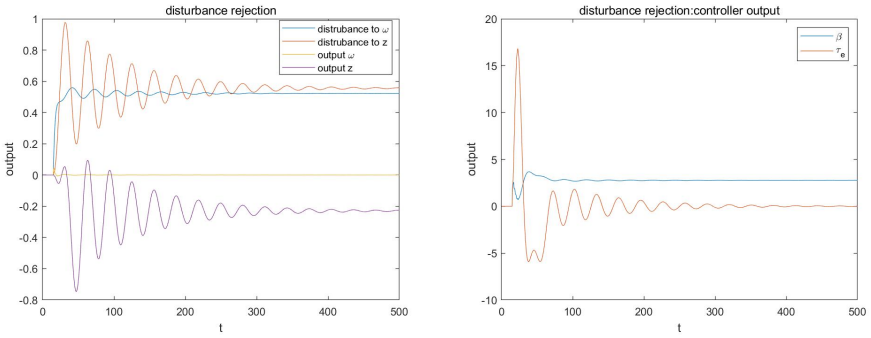

(a)disturbance and FWT output signals. (b)controller output

Figure 23: disturbance rejection.

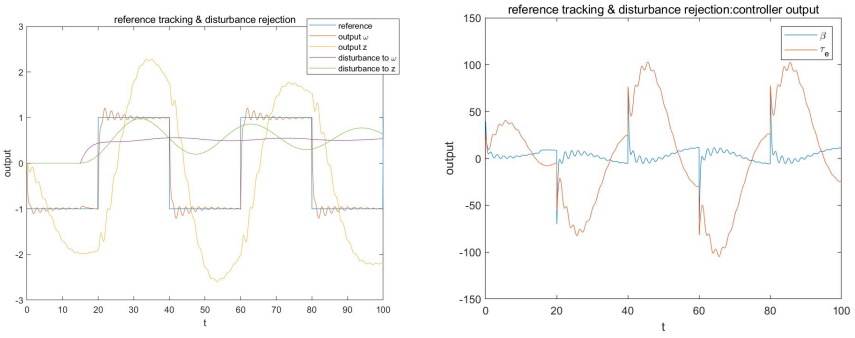

(a)reference, disturbance, FWT signals. (b)controller output

Figure 24: reference tracking(non-constant) and disturbance rejection.

power produced by wind turbine, torque τ_e is suitable for offsetting high-frequency changes in wind speed because blade pitch cannot

change so fast. For low-frequency control, blade pitch angle β is desired one and it can guarantee the power production does not changed by regulating the value of β.

4.1 Generalized Plant

The block diagram is shown in figure 25. In this model,

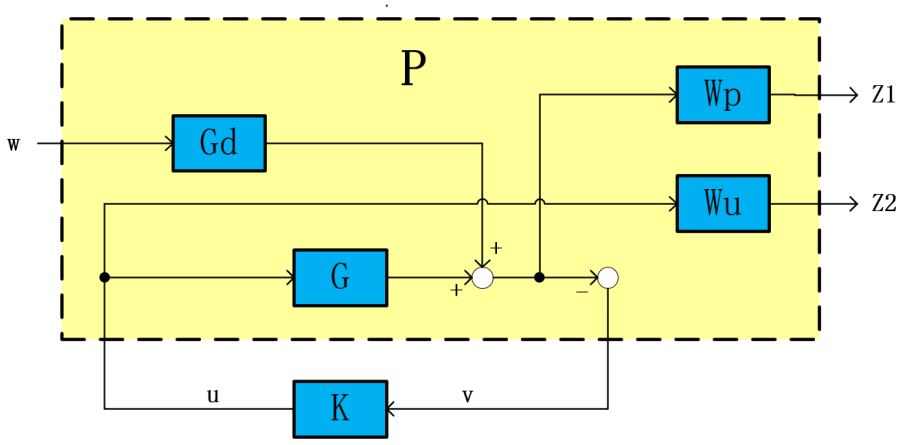

Figure 25: Model of the floating wind turbine and controller with mixed sensitivity.

(1) ω is an 1-dimension exogenous input.

(2) W_p, G_d are 1×1 transfer function.

(3) W_u, G, K are 2×2, 1×2 and 2×1 transfer function matrix.

(4) z_1, z_2 are 1-dimension and 2-dimension exogenous outputs.

(5) u and v are 2-dimension control signals and 1-dimension output signals respectively.

Overall, the plant has three inputs and four outputs.

4.2 Weight design

4.2.1 W_p design

Formula 12 is still selected to design weight W_p. In this case, a bandwidth at around π is expected, so w_B^* is chosen to be equal to

π. A and M keep unchanged. The bode diagram of $1/W_p$ is shown in figure 26.

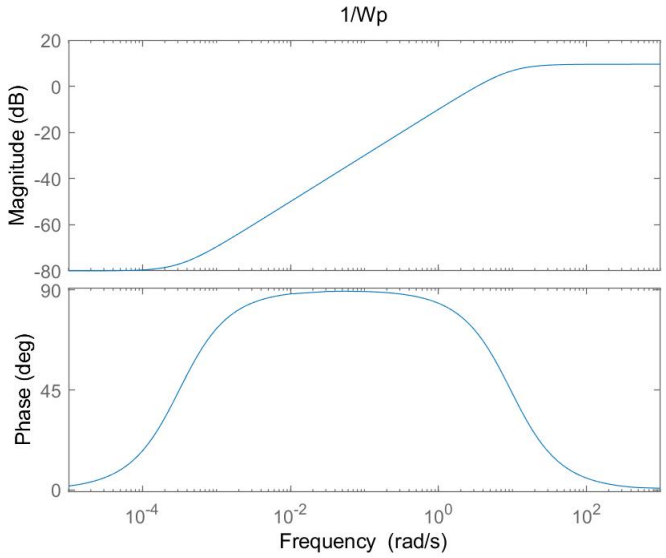

Figure 26: $\frac{1}{W_p}$ design.

4.2.2 W_u design

The low frequent part of the typical wind profile has a period of around 1000 seconds, which is approximately equal to 0.0063rad/s, and the blade pitch is used for low-frequency input (<0.5 Hz), so the frequency of signal β can not exceed πrad/s. Based on that, a weight $W_u(1,1)$ is required to have a low penalty when frequency is less than $\pi rad/s$ and a high penalty when frequency is more than this frequency. By contrast, input signal τ_e is only used to eliminate high frequency disturbance, so a weight $W_u(2,2)$ is required to attenuate low-frequency (at least 0.0063rad/s) disturbance response of τ_e and augment its response to high-frequency disturbance. In order to improve performance of differentiating low-frequency and high-frequency, a steeper slope is expected at the turning point of amplitude. Therefore, a second-order weight is preferred and adopted in this design.

After tuning the parameter and simulating multiple times, the final designed weight is shown in formula 21 and figure 27. From this designed weight, it can be noticed that the controller output β is designed to have high gain (40 db) for low-frequency disturbance, and

the gain starts to decrease when the frequency is more that 0.1rad/s and reaches its lowest value (-40 db) at around 10rad/s. While $1/W_u(2,2)$ reflects that the signal τ_e is expected to have an opposite response character to disturbance (-40 db when freq<0.01rad/s and 40 db when freq>10rad/s).

$$W_u = \begin{bmatrix} \frac{100(s+0.1)^2}{(s+10)^2} & 0 \\ 0 & \frac{0.01(s+1)^2}{(s+0.01)2} \end{bmatrix} \tag{21}$$

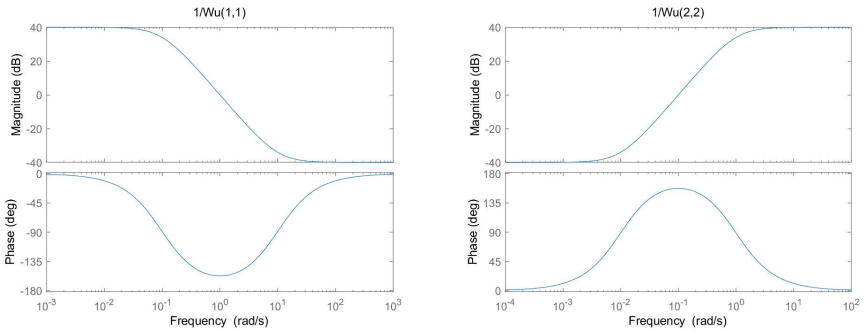

(a) $\frac{1}{W_u(1,1)}$ design result. (b) $\frac{1}{W_u(2,2)}$ design result.

Figure 27: W_u design.

4.3 Implement controllers with weights

By using matlab command **hinfsyn()**, the controllers with these weights above is synthesized. The controllers bodes versus their weights and the sensitivity function with respect to its weight shown in figure 28 and 29 respectively.

From these figures we can find that the controllers and sensitivity function bode curves are not fully bounded by their designed weights. In figure 29, the bode curve of sensitivity function shows a notch, which means the desired bandwidth can not be achieved. In figure 28(a), the bode diagram of β crosses the bound at around 1 10 rad/s, which means it may has slight response when disturbance frequency is larger than 0.5Hz. Finally, the curve of τ_e exceeds the bound at whole low-frequency area, but the gain is still -25.5, which means the response is still attenuated at this frequency.

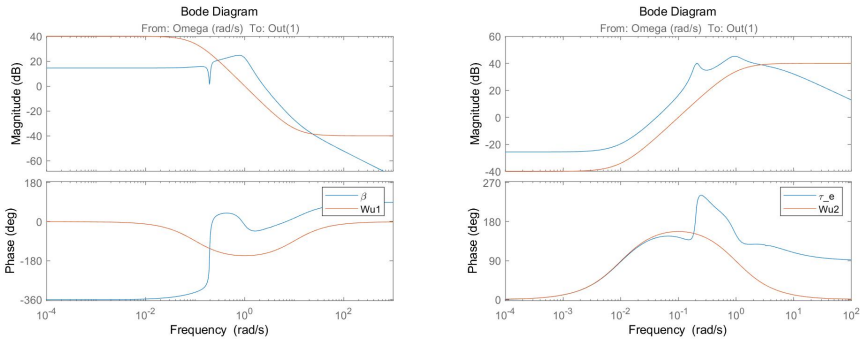

(a)β versus its weight. (b)τ_e versus its weight.

Figure 28: controllers bodes versus their weight.

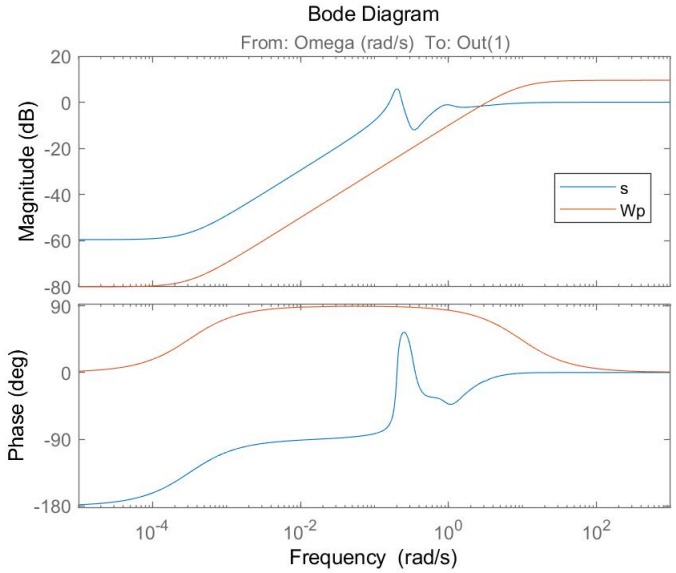

Figure 29: bode diagram for S and its weight.

4.4 Simulation with windspeed data

The system structure implemented controllers with weights in the simulink is shown in figure 30. From figures 31, 32 and 33, we can notice that the controller output β is mainly used to eliminate low-frequency disturbance and τ_e is to cancel out high-frequency disturbance. The controller for τ_e works as expected, namely, only shows a high-frequency response. While the signal β shows a slightly high-frequency component in both figures 31 and 33, the reason is that the frequency response of β exceeds its bound at around 1

rad/s, which has been mentioned in 4.3.

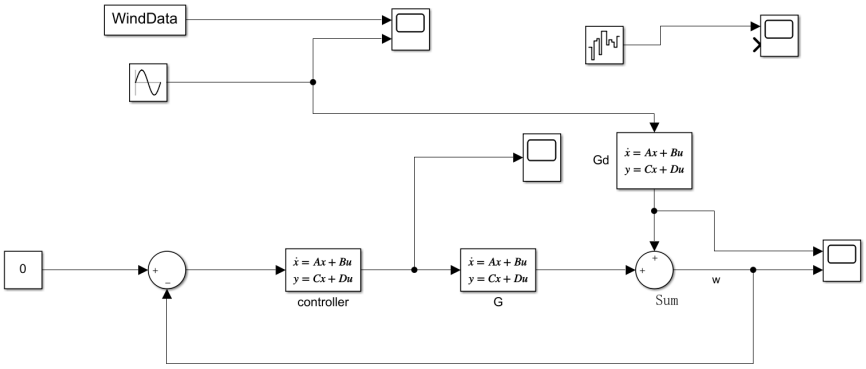

Figure 30: system structure.

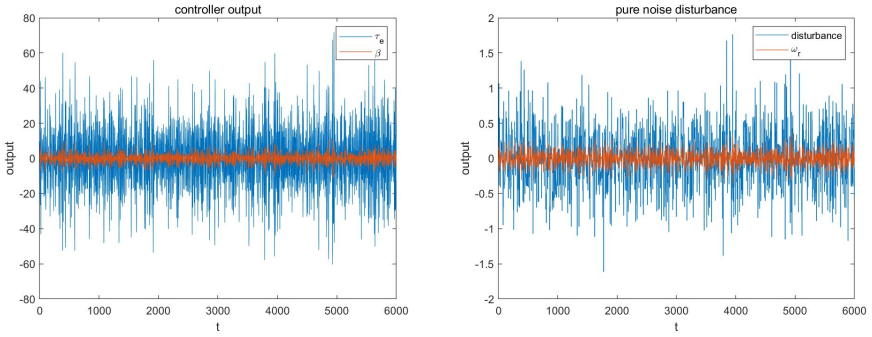

(a)controller output. (b)disturbance and output ω_r.

Figure 31: pure noise disturbance.

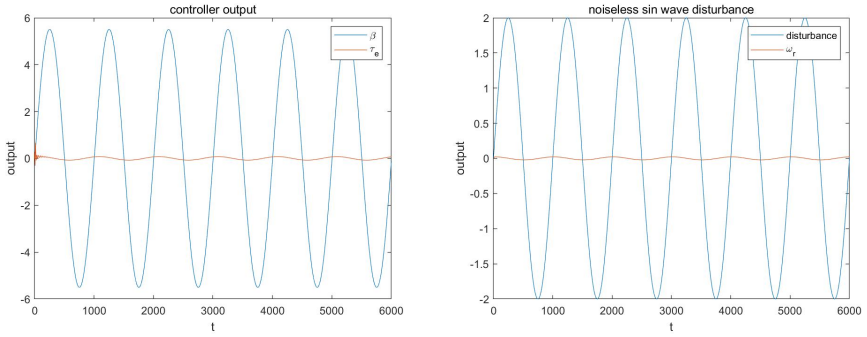

(a)controller output. (b)disturbance and output ω_r.

Figure 32: noiseless sin wave disturbance.

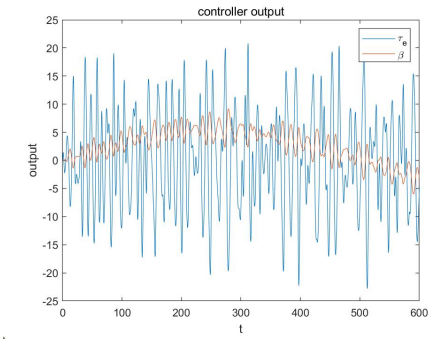

(a)controller output.

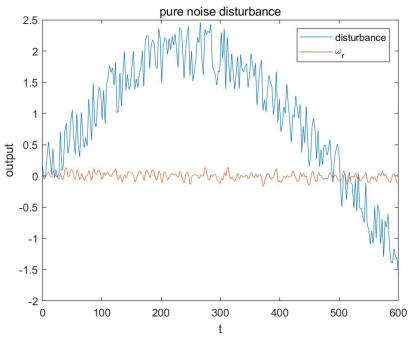

(b)disturbance and output ω_r.

Figure 33: theoretical wind disturbance.

References

[1] Robust Control (SC42145). (2022, October 17). Retrieved from https://brightspace.tudelft.nl/d2l/le/content/501018/Home

[2] Multivariable Feedback Control. Siguird Skogestad and Ian Postlethwaite. Second edition. ISBN: 978-0-470-01168-3.